

Aviation 2006 NO_x-induced effects on atmospheric ozone and HO_x in Community Earth System Model (CESM)

A. Khodayari¹, S. Tilmes³, S. C. Olsen², D. B. Phoenix², D. J. Wuebbles², J.-F. Lamarque³, C.-C. Chen³

[1] {Department of Civil and Environmental Engineering, University of Illinois at Urbana-Champaign, Urbana, IL 61801, USA}

[2] {Department of Atmospheric Sciences, University of Illinois at Urbana-Champaign, Urbana, IL 61801, USA}

[3] {National Center for Atmospheric Research, Boulder, CO, USA}

Correspondence to: Donald J. Wuebbles (wuebbles@illinois.edu)

Abstract

The interaction between atmospheric chemistry and ozone (O₃) in the upper troposphere and lower stratosphere (UTLS) presents a major uncertainty in understanding the effects of aviation on climate. In this study, two configurations of the atmospheric model from the Community Earth System Model (CESM), CAM4 and CAM5, are used to evaluate the effects of aircraft nitrogen oxide (NO_x=NO+NO₂) emissions on ozone and the background chemistry in the UTLS. CAM4 and CAM5 simulations were both performed with extensive tropospheric and stratospheric chemistry including 133 species and 330 photochemical reactions. CAM5 includes direct and indirect aerosol effects on clouds using a modal aerosol module (MAM) whereby CAM4 uses a bulk aerosol module, which can only simulate the direct effect. To examine the accuracy of the aviation NO_x induced ozone distribution in the two models, results from the CAM5 and CAM4 simulations are compared to ozonesonde data. Aviation NO_x emissions for 2006 were obtained from the AEDT (Aviation Environmental Design Tool) global commercial aircraft emissions inventory. Differences between simulated O₃ concentrations and ozonesonde measurements averaged at representative levels in the

1 troposphere and different regions are 13% in CAM5 and 18% in CAM4. Results show a
2 localized increase in aviation induced O₃ concentrations at aviation cruise altitudes that
3 stretches from 40°N to the North Pole. The results indicate a greater and more disperse
4 production of aviation NO_x-induced ozone in CAM5, with the annual tropospheric mean O₃
5 perturbation of 1.2 ppb (2.4%) for CAM5 and 1.0 ppb (1.9%) for CAM4. The annual mean O₃
6 perturbation peaks at about 8.2 ppb (6.4%) and 8.8 ppb (5.2%) in CAM5 and CAM4,
7 respectively. Aviation emissions also result in increased OH concentrations and methane
8 (CH₄) loss rates, reducing the tropospheric methane lifetime in CAM5 and CAM4 by 1.69%
9 and 1.40%, respectively. Aviation NO_x emissions are associated with an instantaneous change
10 in global mean short-term O₃ radiative forcing (RF) of 40.3 and 36.5 mWm⁻² in CAM5 and
11 CAM4, respectively.

12 **1 Introduction**

13 The aviation industry has grown rapidly since its nascence, at a rate of 9% per year for
14 passenger traffic between 1960 and 2000 (IPCC, 1999) and is one of the fastest growing
15 transportation sectors (IPCC, 2007). Despite several international economic and other setbacks
16 over the last few decades, including large price increases for fuel, and a global recession, the
17 aviation industry continues to experience growth. The 2013 FAA forecast calls for an annual
18 average increase of 2.2% per year in U.S. passenger carrier growth over the next twenty years.
19 The growth is predicted to be slightly greater for the first five years under the assumption of a
20 faster U.S. economic growth rate (FAA, 2013). As such, it is important to assess the potential
21 impacts that aviation will have on future climate.

22 Aviation affects climate in various ways. The main concerns to climate result from the
23 emissions of carbon dioxide (CO₂) and nitrogen oxides (NO_x=NO+NO₂), which influence the
24 gas-phase and aerosol chemistry. Other aviation induced impacts result from the emissions of
25 H₂O, and the emission of sulfate and soot particles, which influence the formation of contrail-
26 cirrus clouds and change the cloudiness by acting as cloud condensation nuclei (e.g., Gettelman
27 et. al., 2012). The resulting effects of these emissions modify the chemical properties of the
28 upper troposphere and lower stratosphere and the cloud microphysics that affect the Earth's
29 climate system radiative forcing. For the majority of these effects, the radiative forcing is

1 positive; however, for sulfate particles—which reflect incoming shortwave radiation, and for
2 the increases in OH concentrations—which reduce the CH₄ concentrations, the radiative
3 forcing is negative (Lee et al., 2009). The indirect effect of sulfate aerosols may, on the other
4 hand, result in a negative radiative forcing via liquid clouds which dominates the warming
5 caused from contrails and black carbon (BC) emissions (Gettelman et al., 2013). This study
6 will focus on the aviation NO_x-induced effects, and particularly the NO_x-induced effect on
7 atmospheric ozone (O₃).

8 There have been many previous studies that examined the effect of aviation NO_x emissions on
9 NO_x-induced O₃ (e.g., Derwent et al., 1999; Fuglestad et al., 1999; Wild et al., 2001;
10 Derwent et al., 2001; Stevenson and Doherty, 2004; Köhler et al., 2008; Hoor et al., 2009;
11 Koffi et al., 2010; Hodnebrog et al., 2011). The aviation NO_x-induced changes in O₃ calculated
12 in these studies varies between 0.46 to 0.90 Dobson units of ozone per TgN per year
13 (DU(O₃)/[TgN/yr]). Other recent studies have examined the factors that control the production
14 of NO_x-induced O₃. Stevenson and Derwent (2009) found that the O₃ and CH₄ response to
15 NO_x emissions varies regionally, and are most sensitive in regions with low background NO_x
16 concentrations. Several studies analyzed the impact of the location and time of the emissions
17 (Derwent et al., 2001; Stevenson et al., 2004). Derwent et al. (2001) analyzed the changes in
18 methane and tropospheric ozone after emitting pulses of NO_x at the surface and upper
19 troposphere in both the northern and southern hemispheres and found that while the changes in
20 methane radiative forcing were dominated by methane emissions, changes in tropospheric
21 ozone radiative forcing were dominated by changes in ozone precursor gases, notably NO_x
22 emissions. Stevenson et al. (2004) looked at the effects of an extra pulse of aviation induced
23 NO_x at four months representing the seasonal cycle. Their results showed a seasonal
24 dependence in the O₃ radiative forcing with a long term net radiative forcing of approximately
25 zero. Wild et al. (2012) examined the impact of solar flux variations while Shine et al. (2005)
26 and Berntsen et al. (2005) investigated the effects of atmospheric mixing. However, as reported
27 in Holmes et al. (2011), model-based estimates of aviation NO_x-induced changes in O₃ vary by
28 up to 100%, largely because of differences between models in the ratios of NO : NO₂ and OH :
29 HO₂, background NO_x levels, location and time of emissions, the amount of sunlight, and in
30 atmospheric mixing (Holmes et al., 2011). Recent studies by Olsen et al. (2013) and Brasseur et

al. (2013) found considerable differences between a set of climate-chemistry models (CCMs) and chemistry transport models (CTMs) in comparisons of the background atmosphere and aviation NO_x-induced changes in ozone.

In this study, we examine the effect of aviation NO_x emissions on the atmospheric concentration of O₃ and hydrogen oxide radicals (HO_x=OH+HO₂) and the reduction of CH₄ lifetime using the latest versions of the atmospheric components of the Community Earth System Model (CESM) model, namely the Community Atmosphere Model with Chemistry, Version 4 (CAM4) and Version 5 (CAM5). We further calculate the radiative forcing associated with the changes in O₃ concentration using the University of Illinois Radiative Transfer Model (UIUC RTM). While the calculated effects in CAM4 and CAM5 provide a new reference for the aviation NO_x-induced effects in comprehensive climate-chemistry models, they also provide a measure for the effects of different oxidative capacity in the models, due to differences in description of the physical processes in the model, and especially due to the different treatment of aerosol processes (see model description).

This paper is organized as follows. The following section provides model description. Section 3 discusses the emissions and simulation setup. Section 4 presents the results and section 5 provides the concluding material.

2 Model Description

CAM4 and CAM5 (Community Atmosphere Model versions 4 and 5) are the atmospheric component models for the Community Earth System Model (CESM) (<http://www.cesm.ucar.edu/>). The details of the physics parameterizations in the CAM4 and CAM5 models have been discussed extensively in other studies before (e.g. Neale et al., 2011; Gent et al., 2011; Lamarque et al., 2012). Briefly, CAM5 has been substantially modified in the representation of physical processes compared to CAM4, including a new shallow convection scheme, and updated planetary boundary layer (PBL) schemes, revised cloud macrophysics scheme, updated radiation scheme (Medeiros et al., 2012). These updates improve the representation of cloud properties and permit assessing the indirect effect of aerosols on clouds, which is not included in CAM4.

Cloud microphysical processes are represented by a prognostic, two-moment formulation for cloud droplets and cloud ice. Mass and number concentrations of cloud droplets and cloud ice follow the Morrison and Gettelman (2008) parameterization. The gamma function is employed to determine liquid and ice particle sizes (Gettelman et al., 2008). The evolution of liquid and ice particles in time is affected by grid-scale advection, convective detrainment, and turbulent diffusion. Activation of cloud droplets is a function of aerosol size distribution, aerosol chemistry, temperature, and vertical velocity (Neale et al., 2011). The cloud macrophysics scheme imposes full consistency between cloud fraction and cloud condensate. Liquid cloud fraction is based on a triangular distribution of total relative humidity. Ice cloud fraction is based on Gettelman et al. (2010) that allows supersaturation via a modified relative humidity over ice and the inclusion of the ice condensate amount. The aerosol-cloud scheme simulates full aerosol-cloud interactions such as cloud droplet activation by aerosols, precipitation processes due to particle size dependence, and explicit radiative interaction of cloud particles (Liu et al., 2012). Further, CAM5 was successfully coupled to the full chemical mechanism and released in CESM 1_2_0 and versions thereafter (as discussed in detail in Tilmes et al., in preparation). Since the coupling of aerosols and chemistry in CAM5 has not been released at the time model runs were performed, a development version of close to CESM1_2_0 release version (cesm1_2_beta08_chem) was used for CAM5 simulations, which includes this coupling. The CESM1_0_3 released version was used for CAM4 simulations. Both models use the same gas-phase chemical mechanisms including tropospheric and stratospheric chemistry with about 133 species and 330 photochemical reactions (Lamarque et al., 2012). A complete list of species and reactions can be found in Lamarque et al. (2012). While the two models use the same gas-phase chemistry, there are differences in aerosol properties, due to the different aerosol treatment in CAM4 and CAM5. CAM4 uses a bulk aerosol module with one lognormal distribution for all aerosols (Lamarque et al., 2012) while CAM5 uses the modal aerosol module (MAM) (Liu et al., 2012). MAM was developed with two versions, one with seven lognormal modes (MAM7) and one with three lognormal modes (MAM3) (Liu et al., 2012). Here, we use the more complete version with seven lognormal modes. MAM7 represents Aitken, accumulation, primary carbon, fine dust and sea salt, and coarse dust and sea salt modes. Within each mode, the mass mixing ratios of the respected aerosols and their number

1 mixing ratios are calculated (Liu et al., 2012). MAM simulates both internal and external
2 mixing of aerosols, chemical and optical properties of aerosols, and various complicated
3 aerosols processes (Liu et al., 2012).

4 The UIUC RTM was used offline to calculate the forcing associated with aviation NO_x-
5 induced short-term O₃. Earlier versions of the UIUC RTM have been used in previous research
6 (e.g., Jain et al., 2000; Naik et al., 2000; Youn et al., 2009; Patten et al., 2011). The UIUC
7 RTM calculates the flux of solar and terrestrial radiation across the tropopause. The solar
8 model includes 18 spectral bins from 0.2 to 0.5 microns and includes absorption by H₂O, O₃,
9 O₂, CO₂, clouds, and the surface. Scattering processes by clouds, gas-phase molecules, and the
10 surface are included as well. The terrestrial radiation calculation uses a narrow band model of
11 absorptivity and emissivity that covers wave numbers from 0 to 3000 cm⁻¹ at a resolution of 10
12 cm⁻¹ for H₂O, CFC-11, and CFC-12, and of 5 cm⁻¹ for all other gases. The infrared absorption
13 parameters for gases are obtained from the HITRAN 2004 database (Rothman et al., 2005).
14 Surface albedo and emissivity are based on observations, while clouds are based on the
15 International Satellite Cloud Climatology Project. The use of the same cloud fields for both
16 CAM4 and CAM5 simulations in the offline radiative forcing calculations ensures that the
17 differences in the calculated change in radiative forcing are due to the differences in chemistry
18 and not due to the differences in cloud fields. A previous study by Conley et al. 2013 shows
19 that using different cloud fields in an offline radiative transfer model makes very little to no
20 difference in the calculated change of radiative forcing for radiative active species.

21 **3 Aviation NO_x Emissions and Simulation Setup**

22 Both models were run at a horizontal resolution of 1.9° latitude x 2.5° longitude and were
23 configured with 56 vertical levels covering from the surface up to ~2 hPa with near tropopause
24 resolution of about 1.3 km. To reduce year-to-year climate variability in the model simulations
25 and to help detect the aviation NO_x signal, specified dynamics (“off-line” mode) simulations
26 were performed. In these simulations, changes in the chemical constituents do not affect the
27 dynamics. The models used the GEOS DAS v5.1 meteorology for the year 2005 (Rienecker et
28 al. 2008) which was the closest available assimilated meteorology data to the year of interest
29 (2006). The aviation emissions for 2006 are from the AEDT aviation emissions analyses

(Wilkerson et al., 2010; Olsen et al., 2012). The background emissions of non-aviation short-lived species (e.g., NO_x, volatile organic compounds (VOCs)) were obtained from the IPCC RCP4.5 scenario for year 2005 (van Vuuren et al., 2011) and both models were run with the same total lighting NO_x values. The monthly surface concentrations of longer-lived species, e.g., CO₂, CH₄, chlorofluorocarbons (CFCs), and nitrous oxide (N₂O), were specified as boundary conditions based on the IPCC RCP4.5 scenario. To analyze the effect of aviation NO_x emissions on the background atmosphere, two simulations are performed in each model. One simulation considers all NO_x emissions including aviation NO_x, and the other simulation has all NO_x emissions but no aviation NO_x (control run). The difference between these two simulations corresponds to the changes induced by aviation NO_x. The simulations were run for 7 years, cycling through the 2005 meteorology, to reach steady-state with data from the 7th year used in this analysis.

Since both models were run with same emissions, same total lighting NO_x values, and with identical meteorological fields with 100% nudging, the differences in the description of aerosols very likely have the largest impact on the chemistry of aviation NO_x-induced effects, while differences in clouds may also contribute to some degree. In particular, differences in the aerosol burden, but especially in the surface area density, that are caused by differences in the aerosol size distribution (effective radius) and mass, have an influence on the heterogeneous chemistry and therefore influence the oxidative capacity of the atmosphere and therefore the chemical composition, as further discussed in Section 4.4. The impact of differences in dynamics is expected to be small, since in both models the horizontal winds, surface fluxes and temperatures were prescribed with GEOS meteorological analysis fields.

4 Results and Discussions

4.1 Chemistry Diagnosis

Previous intercomparisons of multiple climate-chemistry models indicated that CAM reasonably simulates the effects of aviation NO_x-induced emissions on distribution of tropospheric O₃ and NO_x (Weber, 2011 and Olsen et al., 2013). However, due to the radiative importance of ozone in troposphere and stratosphere and in relation to differences in aerosols

1 treatment between the two model configurations used in this study, simulated ozone in the
2 control runs at representative altitudes is evaluated using an ozonesonde climatology (Tilmes et
3 al., 2012). This climatology includes observations for the years 1995-2011 and covers averaged
4 ozone profiles for 41 different ozonesonde stations that are grouped into 12 regions. For our
5 comparisons, we evaluate ozone at four pressure levels covering the troposphere and lower
6 stratosphere (50, 250, 500, and 900 hPa) over the 12 areas, which are grouped into three larger
7 regions (Tropics, Mid-Latitudes, and High Latitudes), as shown in Figure 1. Model results are
8 interpolated horizontally to all the stations within each region, and averaged over each region.
9 The comparison between model and observations is illustrated in Taylor-like diagrams for each
10 of the corresponding pressure levels and regions. A slightly different version of CAM4
11 including chemistry has been previously tested against ozone observations as well as the
12 observations of other major atmospheric compounds (e.g., Lamarque et al., 2012).

13 The two model versions are in good agreement at 50 hPa and agree within 10% with the
14 observed values for the mid- and high latitudes, which is the range of the uncertainty of the
15 observations, besides for Japan (deviations to observations are around 15%) and for the SH
16 Polar region for CAM4. The seasonal cycle is well reproduced. The models overestimate the
17 observed ozone concentration in the Tropics by 25 to 50%, with a poor description of the
18 seasonal cycle, especially for CAM5.

19 At 250 hPa, both models reproduce high latitude ozone observations within 25% and show a
20 reasonable agreement with the seasonal cycle. In the Tropics and mid-latitudes, the model
21 largely overestimates ozone, especially for Japan and the SH and most of the tropical stations.
22 The overestimate of ozone in the mid-latitudes and tropics in CAM4 was also found in
23 Lamarque et al. (2012), who noted that this result is an indication of a model estimated
24 tropopause that is lower than observed and possibly too much transport of ozone into the
25 troposphere.

26 Of the four pressure levels studied, the models most accurately simulate ozone at the 500 hPa
27 level. The absolute difference in generated ozone is within 11.7% for both models, which is
28 within the variability of the observations. CAM4 slightly overestimates ozone at all but one
29 location. Overall, CAM5 appears to perform better than CAM4 due to a lower percent

1 difference in ozone (6.0% in CAM5 compared to 11.7% in CAM4). The seasonal cycle is
2 simulated reasonably well for both models, with a correlation coefficient of 0.80 for CAM5 and
3 0.82 for CAM4.

4 On average, both models perform well in the boundary layer (900 hPa), although there are
5 several outliers. Both models overestimate the ozone concentration in the Western Europe and
6 Canada regions. On the other hand, both models underestimate ozone in the SH Mid-Latitude
7 and SH Polar regions. At all other locations, ozone agrees well with observations. The relative
8 bias is lower in CAM5 (10.0% compared to 15.7% in CAM4), indicating a better representation
9 of ozone by CAM5. Additionally, with the exception of the Equatorial Americas region in
10 CAM4 and the Japan region for both models, the seasonal correlation is excellent (0.81 in both
11 CAM5 and CAM4).

12 Overall, both models simulate ozone more accurately in the troposphere than in the UTLS and
13 stratosphere and overestimate ozone in the tropical transition layer. The simulated seasonal
14 cycle in CAM4 is slightly better than in CAM5 in comparison to observations.

15 Comparisons of O₃, NO_x, HNO₃, PAN, as well as CO to aircraft observations between 2-7 km
16 (Emmons et al., 2000; Tilmes et al., in preparation), where the majority of the observations
17 were taken is also shown in Figure 2, both the control and perturbed simulations.

18 In comparison to aircraft data, ozone is slightly overestimated in the tropics, especially for the
19 perturbed simulations, in agreement with ozonesonde observations, while there is reasonable
20 agreement in mid- and high latitudes. Both model versions simulate the regional differences in
21 NO_x in comparison to available aircraft observations reasonably well, but NO_x is slightly
22 underestimated by all model simulations is summer in NH mid-latitudes. Both model versions
23 overestimate PAN and HNO₃ in tropics and mid-latitudes and high latitude in spring. Model
24 differences between CAM4 and CAM5 are within the variability of the observations. CO is
25 underestimated in both model versions, with much larger deviations from the observations for
26 CAM5 than CAM4. This points to a significant overestimation of OH in CAM5, as also
27 indicated by the smaller methane lifetime in CAM5 compared to CAM4. The increase in NO_x
28 due to aircraft emissions does not affect NO_x, NO_y, and CO very much in the altitude

considered. However, ozone is slightly increased in the perturbed case for both CAM4 and CAM5.

4.2 Spatial distribution of NO_x emissions

The AEDT NO_x emission data used as the input to the model runs had an hourly temporal resolution. The spatial distribution of aviation NO_x emissions for 2006 is shown in Figure 3 which amounts to 2.7 Tg (NO₂)/yr. As in Figure 3, the largest intensity of NO_x emissions is in the eastern United States, eastern Asia, and Europe. The local maximum in the eastern U.S. contributes approximately 0.0136 Tg to the global emissions of NO₂ while the local maximum in Europe contributes 0.0154 Tg. Additionally, the peak value in Asia contributes 0.0123 Tg to the global total. These values represent the maximum emissions from a single grid cell. The main source of NO_x emissions occur between 30° and 60°N latitude.

Figure 4 shows the seasonal distribution of aviation NO_x emissions from 2006. As shown in Figure 4, aviation NO_x emissions have a different seasonal distribution with the highest amount of emissions released in the summer, due to increased air traffic in those months.

4.3 Ozone production and loss

The NO_x-induced changes in tropospheric ozone are complicated by two stages, a short-term increase in O₃ concentrations associated with a positive forcing, and a long-term reduction of O₃ concentrations tied to the aviation induced methane decrease. This long term-reduction is associated with negative forcing (Wild et al., 2001; Stevenson et al., 2004). Since our simulations were performed with fixed CH₄ mixing ratios at the boundary layer, the calculated changes in O₃ concentration are the short-term changes.

Figure 5 shows the aviation NO_x-induced annual vertical profile of short-term O₃ production and loss as calculated by CAM5 (red) and CAM4 (blue). Both models show the maximum rate of ozone production peaking in the upper troposphere/lower stratosphere (UTLS) region where the greatest amount of aircraft induced NO_x emissions occur.

As we analyze the results from the model runs, we use the following chemical reactions for ozone production in the troposphere (Sillman, 2012):

P1	$VOC + OH \xrightarrow{O_2} RO_2 + H_2O$
P2	$CO + OH \xrightarrow{O_2} HO_2 + CO_2$
P3	$RO_2 + NO \xrightarrow{O_2} secondary\ VOC + HO_2 + NO_2$
P4	$HO_2 + NO \rightarrow OH + NO_2$
P5	$NO_2 + h\nu \rightarrow NO + O$
P6	$O + O_2 + M \rightarrow O_3 + M$

Ozone destruction in the troposphere, on the other hand, is given by the following reactions (Sillman, 2012):

L1	$NO + O_3 \rightarrow NO_2 + O_2$
L2	$O_3 + h\nu \xrightarrow{H_2O} 2OH + O_2$
L3	$HCHO + h\nu \xrightarrow{2O_2} 2HO_2 + CO$
L4	$HO_2 + HO_2 \rightarrow H_2O_2 + O_2$
L5	$RO_2 + HO_2 \rightarrow ROOH + O_2$
L6	$OH + NO_2 \rightarrow HNO_3$

The impact of aviation induced NO_x on ozone results in a net increase in the rate of ozone production with a maximum around 250hPa, and a net decrease in the rate of ozone production below 450 hPa. Within the UTLS region, the rate of ozone loss decreases due to the increase in HO₂ (Figure 9, as discussed below) reacting with NO (as in equation P4). This process creates NO₂ which further increases O₃ production (by equations P5 and P6). Part of the excess ozone that is created in the UTLS region is transported to lower altitudes. As shown in Figure 5, the rate of ozone loss peaks around 500 hPa. As described by equation L2, at this altitude, excess ozone transported from the UTLS region in the presence of water vapor reacts to form HO_x, increasing ozone loss. Additional reductions in the net O₃ production are caused

1 by the increased reaction of HO_x with NO_x near the surface, resulting in the conversion of NO_x
2 to HNO₃ (equation L6).

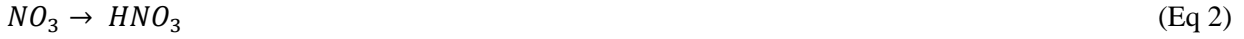
3 While the patterns of the changes in the simulated ozone production and loss agree well
4 between the models and with previous studies (Köhler et al., 2008), there are differences
5 between CAM4 and CAM5 in the magnitudes. Compared to CAM4, overall ozone production
6 and loss are larger in CAM5, due to the differences in OH between the models. The net rate of
7 ozone production in CAM5 is higher at cruise altitudes and slightly lower at lower altitudes.
8 The maximum net production of ozone is 1.1×10^{20} molecules.s⁻¹.Pa⁻¹ in CAM5 and 1.0×10^{20}
9 molecules.s⁻¹.Pa⁻¹ in CAM4. CAM4 estimates a maximum rate of production at 1.2×10^{20}
10 molecules.s⁻¹.Pa⁻¹ while CAM5 estimates a rate of 1.4×10^{20} molecules.s⁻¹.Pa⁻¹. At lower
11 altitudes, CAM5 gives a greater rate of ozone loss than CAM4. Both models show a peak in the
12 ozone loss rate around 600 hPa with values of about 0.5×10^{20} molecules.s⁻¹.Pa⁻¹ in CAM5, and
13 about 0.4×10^{20} molecules.s⁻¹.Pa⁻¹ in CAM4. Overall, as found in Figure 1 (as confirmed
14 through comparisons with ozonesonde data) and shown in Figure 5, CAM5 is more efficient in
15 producing ozone than CAM4 in most of the atmosphere.

16 **4.4 Global burdens**

17 Table 1 compares the annual mean tropospheric burden of HO_x, NO_x, gaseous NO_y and the
18 ratios of OH : HO₂ and NO_x : NO_y in both CAM4 and CAM5 for both the control run and
19 aviation NO_x-perturbed run. The comparison of the burdens presented in Table 1 indicates that
20 the background atmosphere is relatively different between the two models (e.g. ~8.1%
21 difference in the background O₃). While such differences seem to be smaller compared to the
22 intermodel uncertainty ($\pm 25\%$) reported in Stevenson et al. (2006), there is about 11.8%
23 difference in the aviation NO_x-induced annual mean tropospheric O₃ response.

24 As shown in Table 1, The ratio of NO_x : NO_y is about 7% higher in CAM5 perturbed run than
25 in CAM4 perturbed run implying a smaller shift of the NO_x : NO_y relationship to NO_y in
26 CAM5. The smaller shift of the NO_x : NO_y relationship to NO_y in CAM5 is tied to
27 heterogeneous reactions and related to less aerosol surface area density in CAM5 compared to
28 CAM4. Under lower aerosol surface area density, heterogeneous reaction can be less effective

in moving NO_x to NO_y and this results in more OH, and shorter CH₄ lifetime (as seen in Table 2). Heterogeneous reactions that are included in CAM chemical mechanism are listed in Eq 1-3.



As such, due to less efficient transfer of NO_x to NO_y in CAM5 compared to CAM4 there is more nitrogen available in its reactive form (NO_x) to trigger the ozone formation reactions in CAM5, resulting in higher aviation NO_x-induced ozone perturbation.

4.5 Ozone

The aviation NO_x-induced ozone perturbation is shown in Figure 6. Model results from CAM5 are shown on the top panel while CAM4 is on the bottom. The left column shows the mean zonal ozone perturbation for January, while the right column shows July. As shown in Figure 6, CAM5 produces a greater amount and wider distribution of ozone in the UTLS region for both months. The pattern and the localized maximum of the ozone perturbation at 200 hPa in the NH are about the same in both CAM4 and CAM5. The tropospheric mean change in O₃ is higher in CAM5 than CAM4 for both January and July. In July, CAM5 generates a tropospheric mean ozone perturbation of 1.16 ppb (compared to 1.0 in CAM4). In January, CAM5 generates a tropospheric mean ozone perturbation of 1.18 ppb (compared to 1.1 in CAM4). Overall, aviation NO_x emissions from the year 2006 yield an annual tropospheric mean O₃ perturbation of 1.2 ppb (2.4%) in CAM5 and 1.0 ppb (1.9%) in CAM4. The annual mean O₃ perturbation peaks at 8.2 ppb (6.4%) in CAM5 and 8.8 ppb (5.2%) in CAM4. Despite the greater production of annual mean O₃ in CAM5, the peak is slightly lower in CAM5 compared to CAM4, since the produced O₃ is more distributed towards the surface in CAM5.

As shown in Figure 6, the UTLS ozone perturbation is much greater in July than in January for both models. This is due to differences in the length of daylight between those months, increased photochemistry, and higher aviation NO_x emissions in July (as shown in Figure 4). The increased daylight allows more photolysis of NO₂ to occur, which generates O₃ (equations

P5 and P6). Also note the differences in ozone perturbations in the lower troposphere between January and July. In the summer, the ozone perturbation at lower altitudes is weaker due to greater surface deposition and also the shorter photochemical lifetime of ozone through increased water vapor (and more HOx giving increased ozone loss) (Hodnebrog et al., 2011). Additionally, both models show the maximum ozone impact increasing towards high latitudes in the NH in July. A similar result was found by Hoor et al. (2009) who showed a maximum zonal mean ozone perturbation centered around 75° N during June.

As shown in both months and models, a mid-latitudinal perturbation extends from 400 hPa down towards the surface. This feature agrees with past studies by Hoor et al. (2009), Koffi et al. (2010), and Hodnebrog et al. (2011). Hoor et al. (2009) notes that this feature is due to more vigorous boundary layer mixing and convective transport into the free troposphere during the summer.

As shown in Figure 7, annual mean column ozone changes are relatively zonally well mixed, however, several ‘hotspots’ in both CAM5 and CAM4 exist just north of the Mediterranean and off the western coast of Europe. A more uniform spread is seen over Europe, the western half of Asia, the Atlantic Ocean and a small strip at about 45°N in the Pacific Ocean. These ‘hotspots’ are stronger in CAM5 and peak at about 2.3 DU compared to 2.1 DU in CAM4. As expected, the ozone impact is very small in the SH. A sharp ozone gradient exists in the NH subtropics, as was also seen in previous studies. The ozone concentration continues to increase, with the maximum values between 30 and 60° N. Hoor et al. (2009) and Hodnebrog et al. (2011) found a similar distribution. Overall, aviation NOx emissions from the year 2006 lead to a 1.0 and 0.9 DU change in annual global mean ozone column in CAM5 and CAM4, respectively.

4.6 HOx

The hydroxyl radical (OH) plays an important role in the creation of atmospheric ozone. It is the primary oxidizing agent of the troposphere, removing greenhouse gases such as CH₄, CO, HCFCs, and others. Production of OH by O₃ is given by equation L2. Figure 8 shows the increase in aviation induced zonal mean annual OH perturbations.

1 Similar to ozone, the impact of aviation emitted NO_x on tropospheric OH production is largest
2 in July. This increase in OH during the summer months is also due to the enhanced
3 photochemistry. Aircraft emissions have the largest zonal mean ozone impact in the UTLS
4 region in mid- and high latitudes in the NH between 40-90°N. However, the OH perturbation is
5 more concentrated south of the O₃ perturbations. The more southern position of OH is due to
6 the increased humidity and the lower solar zenith angle, which are essential to produce the
7 excited oxygen atom (O(¹D)) and hence higher OH concentrations. This result agrees well with
8 recent studies by Hoor et al. (2009) and Hodnebrog et al. (2011). Additionally, there is a greater
9 perturbation of OH extending towards the surface over mid-latitudes than there was of O₃. This
10 is due to the increased production of HO_x in the mid-troposphere triggered by O₃ photolysis and
11 the presence of water vapor. Additionally, both models show OH perturbations extending from
12 400 hPa down to the surface above 40°N. This feature is much weaker in January because the
13 UV actinic flux necessary for OH production is much smaller in the NH.

14 Between the two models, the OH concentration is higher in CAM5 than CAM4. This is a result
15 of higher O₃ production in CAM5. In July, the CAM5 aviation NO_x-induced tropospheric
16 mean OH perturbation is 1.2×10^4 molecules.cm⁻³ (compared to 9.1×10^3 in CAM4). In January,
17 the CAM5 aviation NO_x-induced tropospheric mean OH perturbation is 9.4×10^3 molecules cm⁻³
18 (compared to 6.4×10^3 in CAM4). Overall, aviation NO_x emissions from the year 2006 lead to
19 an annual tropospheric mean OH perturbation of 1.1×10^4 molecules.cm⁻³ in CAM5 and 7.8×10^3
20 molecules.cm⁻³ in CAM4.

21 Figure 9 shows the CAM4 and CAM5 HO₂ perturbations due to aviation NO_x emissions.
22 Areas that experience an increase in HO₂ concentrations are shown in red and areas that
23 experience a decrease in HO₂ are in blue. Increases in NO_x emissions from aviation increases
24 OH levels by shifting the HO_x balance in favor of OH production, given by equation P4
25 (Stevenson et al., 2004; Berntsen et al., 2005; Köhler et al., 2008). This process results in HO₂
26 loss at cruise altitudes. As expected, the areas of HO₂ loss correspond to the areas that
27 experienced an increase in OH concentrations.

28 In January, there is a greater rate of HO₂ consumption in the UTLS region in CAM5 than there
29 is in CAM4 due to higher OH production. Following equation P4, this HO₂ reacts with aircraft

emitted NO to give OH and NO₂. Similarly, the rate of HO₂ consumption is also greater in the UTLS region during July in CAM5 as well. When comparing Figure 9 with Figure 8, the locations of maximum HO₂ loss correspond with the locations of maximum OH concentration changes, indicating that reaction P4 is a significant reaction in OH production in the UTLS region. At lower altitudes in July, the transported ozone is photolyzed in the presence of water vapor, thus increasing OH, and subsequently HO₂.

4.7 CH₄

The hydroxyl radical OH is the largest sink of CH₄ in the atmosphere. As the OH concentration is effected by aircraft emissions, so is the methane concentration and its lifetime.

Figure 10 shows the aviation induced annual zonal averaged CH₄ loss rate for CAM5 (left) and CAM4 (right). In both CAM5 and CAM4, the change in methane loss is mostly confined to the NH at a location south of the OH perturbation (between 0-30°N). This predominately occurs due to the increase in the methane-OH reaction rate constant with higher temperatures at lower altitudes. As such, in both models the position of the maximum CH₄ loss is below the cruise altitude. As shown in Figure 10, the CH₄ loss is higher in CAM5 than CAM4 due to the higher production of aviation induced OH in CAM5. Table 2 shows the reduction in methane lifetimes as calculated for both CAM4 and CAM5.

Table 2 shows the global annual average CH₄ lifetimes against reaction with OH, as calculated by CAM4 and CAM5 for the background (control) run and the NO_x-perturbed run. It is noted that same as most other models (Voulgarakis et al., 2013 and Naik et al., 2013) the calculated lifetimes here are shorter than the CH₄ lifetime derived based on Methyl chloroform analysis (Prather et al., 2012). The change in CH₄ lifetime is also presented as the percent change in lifetime. The reduction in CH₄ lifetime calculated in CAM5 and CAM4 is 1.69% (2.50%/ [TgN/yr]) and 1.40% (1.71%/ [TgN/yr]), respectively, excluding the feedback of changes in methane concentration on its own lifetime (e.g. Prather 1994; Fuglestedt et al. 1999; Wild et al. 2001 and IPCC 2007). The CAM4 reduction in CH₄ lifetime falls within the -1.4±0.4 (%/[TgN/yr]) to -1.6±0.37 (%/[TgN/yr]) range reported by Hodnebrog et al. (2011). The CAM5 simulated change in CH₄ lifetime is greater than the upper range reported by

Hodnebrog et al. (2011). Inclusion of the aviation induced methane feedback on its lifetime further decreases the lifetime by a factor of 1.4 (IPCC, 2001). The greater reduction of the CH₄ lifetime in CAM5 is the result of a greater increase in the aviation induced OH concentration in CAM5.

4.8 Aviation NO_x-Induced Ozone Radiative Forcings

The aviation NO_x-induced short-term O₃ RFs were calculated as the difference of the radiation imbalance between the NO_x-perturbed and control simulations at the tropopause calculated with the UIUC RTM, excluding the effects of stratospheric adjustment. Figure 11 shows the yearly averaged short-term ozone RF for CAM5 (left) and CAM4 (right). Both models show the greatest RF in the NH between 30-60°N with highest RF changes over Southern Europe and the Middle East. As expected, the O₃ RF from aviation is low in the SH. The greatest RF values in the SH are over the SH tropical Pacific Ocean and are most likely due to air traffic between Australia and the United States. Interestingly, radiative forcing values over Asia are relatively low, given the amount of NO_x emissions from this area. Additionally, it appears that the maximum radiative forcing from Europe's emissions has shifted to the Mediterranean, indicating that these aircraft emissions have a maximum impact downwind of the source. These results agree well with Hodnebrog et al. (2011).

The associated global mean short-term ozone RF is 40.3 and 36.5 mWm⁻² in CAM5 and CAM4, respectively. CAM5 has a greater annual ozone RF, due to the greater ozone perturbation, which largely accounts for the differences in radiative forcings. It is noted that Fuglestad et al. 2008 compares the aviation contribution in changing the radiative forcing to the contribution from other transportation sectors.

5 Conclusion

CAM5 and CAM4 simulate background ozone to within 13% and 18% (on average and at all the locations), respectively, compared to ozonesonde datasets. Based on the comparison with ozonesonde observations, CAM5 was more accurate at determining the ozone distribution in the troposphere and lower stratosphere.

1 Aviation induced O_3 is higher in CAM5 than CAM4 with an annual tropospheric mean O_3
2 perturbation of 1.2 ppb (2.4%) in CAM5 and 1.0 ppb (1.9%) in CAM4. In July, CAM5
3 generates an aviation NO_x -induced tropospheric mean ozone perturbation of 1.16 ppb
4 (compared to 1.0 in CAM4) with a corresponding value of 1.18 ppb in Jan (compared to 1.1 in
5 CAM4).

6 As found in previous studies, the maximum effect from aircraft NO_x emissions on ozone is in
7 the NH Upper Troposphere/Lower Stratosphere region. This is due to the high frequency of
8 subsonic aircraft flying in this region. The aircraft-induced ozone perturbation is greater in the
9 NH summer due to the enhanced photochemistry. In January, the ozone perturbation mixes
10 more towards the surface due to the longer photochemical lifetime of ozone and the slower
11 surface deposition rate than in July.

12 The hydroxyl perturbations are located to the south and at a lower altitude than the position of
13 the maximum change in ozone. This is due to the lower zenith angle and increased humidity
14 which are essential to produce the excited oxygen atom ($O(^1D)$) and hence higher OH
15 concentrations. Overall, the aviation NO_x -induced change in OH is higher in CAM5 in
16 accordance with higher ozone production. The induced changes in OH concentrations increase
17 the methane (CH_4) loss rate and reduce its lifetime by 1.69% and 1.40% in CAM5 and CAM4,
18 respectively.

19 Results indicate a global mean O_3 RF of 40.3 and 36.5 mWm^{-2} in CAM5 and CAM4,
20 respectively. Both models agree that the maximum O_3 radiative forcing is between 30-60°N.
21 However, it is interesting to note that it appears that the maximum RF is downwind of a local
22 maximum NO_x source.

23 This study is the first evaluation of aviation NO_x effects in CAM5 which simulates the size
24 distribution of aerosols, both internal and external mixing of aerosols, chemical and optical
25 properties of aerosols. It is noted that while the simulated change in ozone is relatively different
26 between the two models, the difference between CAM4 and CAM5 ozone responses is
27 considerably smaller than the current estimates of the uncertainty in aviation effects on ozone.
28 The difference in aviation NO_x -induced effects between the two models is related to the

1 difference between the two models configuration used in this study (i.e. difference in aerosols
2 treatment). More detailed analyses are required to explore the impact of the differences in the
3 representation of the background atmosphere and treatment of aerosols processes on aviation
4 NO_x-induced effects to a greater extent.

5 **Acknowledgments**

6 The authors would like to thank the Federal Aviation Administration, Aviation Climate Change
7 Research Initiative (ACCRI) for support under Contract #: 10-C-NE-UI amendment 001 and
8 The Partnership for Air Transportation Noise and Emissions Reduction (PARTNER). The
9 opinions, findings, and conclusions or recommendations expressed in this material are those of
10 the authors and do not necessarily reflect the views of ACCRI, PARTNER, or the FAA. This
11 work was partially supported by the U.S. Department of Transportation, the Illinois Department
12 of Transportation and the Transportation Research and Analysis Computing Center. The
13 authors would like to thank the National Center for Atmospheric Research (NCAR) for the
14 support with computing time and NCAR is supported by the National Science Foundation
15 (NSF). The CESM project (which includes CAM4, CAM5 and CAM-chem) is supported by the
16 National Science Foundation and the Office of Science (BER) of the U. S. Department of
17 Energy. The authors would like to also thank Dr. Francis Vitt (NCAR) for his help in
18 integrating aviation NO_x emissions into CAM5.

19 **References**

20 Arnold, F., Scheid, J., Stilp, T., Schlager, H., and Reinhardt, M. E.: Measurements of jet
21 aircraft emissions at cruise altitude I: The odd-nitrogen gases NO, NO₂, HNO₂ and HNO₃,
22 Geophysical Research Letters, 19, 2421-2424, 1992.

23
24 Beck, J. P., Reeves, C. E., De Leeuw, F. A., and Penkett, S. A.: The effect of aircraft emissions
25 on tropospheric ozone in the northern hemisphere, Atmospheric Environment, Part A. General
26 Topics, 26, 17-29, 1992.

1 Berntsen, T. K., Fuglestad, J. S., Joshi, M. M., Shine, K. P., Stuber, N., Ponater, M., Sausen,
2 R., Hauglustaine, D. A., and Li, L.: Response of climate to regional emissions of ozone
3 precursors: Sensitivities and warming potentials, *Tellus B*, 57B, 283 – 304, 2005.

4
5 Borucki, W. J., Whitten, R. C., Watson, V. R., Woodward, H. T., Riegel, C. A., Capone, L. A.,
6 and Becker, T.: Model predictions of latitude-dependent ozone depletion due to supersonic
7 transport operations, *AIAA Journal*, 14 =, 1738-1745, 1976.

8
9 Brasseur, G. P., Müller, J.-F., and Granier, C.: Atmospheric impact of NO_x emissions by
10 subsonic aircraft: A three-dimensional model study, *Journal of Geophysical Research*, 101
11 (D1), 1423–1428, 1996.

12
13 Brasseur, P. G., Weber, B., Damoah, R., Douglass, A. R., Jacobson, M. Z., Lee, H., Liang, Q.,
14 Olsen, S. C., Oman, L. D., Ott, L., Pawson, S., Selkirk, H., Sokolov, A., Stolarski, R. S.,
15 Unger, N., and Wuebbles, D. J.: Model intercomparison of ozone sensitivity to NO_x emissions
16 in the vicinity of the extratropical tropopause, *Geophysical Research Letters*, submitted, 2013.

17
18 Climatic Impact Assessment Program (CIAP), Report of findings, The effects of stratospheric
19 pollution by aircraft, Rep. DOT-TST-75-50, U.S. Dep. of Transp., Washington, D.C., 1974.

20
21 Collins, W. J., Bellouin, N., Doutriaux-Boucher, M., Gedney, N., Halloran, P., Hinton, T.,
22 Hughes, J., Jones, C. D., Joshi, M., Liddicoat, S., Martin, G., O'Connor, F., Rae, J., Senior, C.,
23 Sitch, S., Totterdell, I., Wiltshire, A., and Woodward, S.: Development and evaluation of an
24 Earth-system model – HadGEM2, *Geoscientific Model Development Discussion*, 4, 997-1062,
25 2011.

26
27 Crutzen, P. J.: SST's: A threat to the Earth's ozone shield, *Ambio*, 1, 1972.

1 Dameris, M., Grewe, V., Köhler, I., Sausen, R., Bruhl, C., Grooss, J. U., and Steil, B.: Impact
2 of aircraft NO_x emissions on tropospheric and stratospheric ozone. Part II: 3-D model results,
3 Atmospheric Environment, 32, 3185–3199, 1998.

4

5 Derwent, R. G.: Two-dimensional model studies of the impact of aircraft exhaust emissions on
6 tropospheric ozone, Atmospheric Environment, 18, 1997-2007, 1982.

7

8 Derwent, R. G., Collins, W. J., Johnson, C. E., and Stevenson, D. S.: Transient behavior of
9 tropospheric ozone precursors in a global 3-D CTM and their indirect greenhouse effects,
10 Climatic Change, 49, 463-487, 2001.

11

12 Emmons, L. K., Walters, S., Hess, P. G., Lamarque, J.-F., Pfister, G. G., Fillmore, D., Granier,
13 C., Guenther, A., Kinnison, D., Laepple, T., Orlando, J., Tie, X., Tyndall, G., Wiedinmyer, C.,
14 Baughcum, S. L., and Kloster, S.: Description and evaluation of the Model for OZone And
15 Related chemical Tracers, version 4 (MOZART-4), Geoscientific Model Development, 3, 43–
16 67, 2010.

17

18 Fitcher, C., Marquart, S., Sausen, R., and Lee, D. S.: The impact of cruise altitude on contrails
19 and related radiative forcing, Meteorologische Zeitschrift, 14, 563 – 572, 2005.

20

21 Flatøy, F., and Hov, Ø.: Three-dimensional model studies of the effect of NO_x emissions from
22 aircraft on ozone in the upper troposphere over Europe and the North Atlantic, Journal of
23 Geophysical Research, 101 (D1), 1401-1422, 1996.

24

25 Fuglestad, J. S., Berntsen, T., Isaksen, I. S. A., Huiting, M., Liang, X.-Z. , and Wang, W.-C.:
26 Climatic forcing of nitrogen oxides through changes in tropospheric ozone and methane; global
27 3D model studies, Atmospheric Environment, 33, 961-977, 1999.

28

1 Fuglestad, J. S., Berntsen T., Myhre G., Rypdal K. and Skeie R. B.: Climate forcing from
2 the Transport Sectors, Proceedings of the National Academy of Sciences (PNAS), vol 105 (no.
3 2), 454-458, 2008.

4
5 Gauss, M., Myhre, G., Pitari, G., Prather, M. J., Isaksen, I. S. A., Berntsen, T. K., Brasseur, G.
6 P., Dentener, F. J., Derwent, R. G., Hauglustaine, D. A., Horowitz, L. W., Jacob, D. J.,
7 Johnson, M., Law, K. S., Mickley, L. J., Müller, J.-F., Plantévin, P.-H., Pyle, J. A., Rogers, H.
8 L., Stevenson, D. S., Sundet, J. K., van Weele, M., and Wild, O.: Radiative forcing in the 21st
9 century due to ozone changes in the troposphere and the lower stratosphere, Journal of
10 Geophysical Research: Atmospheres, 108 (D9), 2003.

11
12 Gauss, M., Isaksen, I. S. A., Lee, D. S., and Søvde, O. A.: Impact of aircraft NO_x emissions on
13 the atmosphere – tradeoffs to reduce the impact, Journal of Atmospheric Chemistry and
14 Physics, 6, 1529-1548, 2006.

15
16 Gent, P. R., Danabasoglu, G., Donner, L. J., Holland, M. M., Hunke, E. C., Jayne, S. R.,
17 Lawrence, D. M., Neale, R. B., Rasch, P. J., Vertenstein, M., Worley, P. H., Yang, Z.-L., and
18 Zhang, M.: The community climate system model version 4, Journal of Climate, 24, 4973-
19 4991, 2001.

20
21 Gettelman, A., Morrison, H., and Ghan, S. J.: A new two-moment bulk stratiform cloud
22 microphysics scheme in the NCAR Community Atmosphere Model (CAM3), Part II: Single-
23 column and global results, Journal of Climate, 21, 3660–3679, 2008.

24
25 Gettelman, A., Liu, X., Ghan, S. J., Morrison, H., Park, S., Conley, A. J., Klein, S. A., Boyle,
26 J., Mitchell, D. L., and Li, J.-LF.: Global simulations of ice nucleation and ice supersaturation
27 with an improved cloud scheme in the Community Atmosphere Model, Journal of Geophysical
28 Research, 115, D18216, doi:10.1029/2009JD013797, 2010.

1 Gettelman, A., Liu, X., Barahona, D., Lohmann, U., and Chen, C.: Climate impacts of ice
 2 nucleation, *Journal of Geophysical Research*, 117, D20201, doi:10.1029/2012JD017950, 2012.
 3
 4 Gettelman, A. and Chen, C.: The climate impact of aviation aerosols, *Journal of Geophysical*
 5 *Research*, 40 (11) (2013), pp. 2785-2789, DOI: 10.1002/grl.50520, 2013.
 6 Hesstvedt, E.: Reduction of stratospheric ozone from high-flying aircraft, studied in a two-
 7 dimensional photochemical model with transport, *Canadian Journal of Chemistry*, 52, 1592-
 8 1598, 1974.
 9
 10 Hodnebrog, Ø., Berntsen, T. K., Dessens, O., Gauss, M., Grewe, V., Isaksen, I. S. A., Koffi, B.,
 11 Myhre, G., Olivie, D., Prather, M. J., Pyle, J. A., Stordal, F., Szopa, S., Tang, Q., Velthoven,
 12 P., Williams, J. E., and Ødemark, K.: Future impact of non-land based traffic emissions on
 13 atmospheric ozone and OH – an optimistic scenario and a possible mitigation strategy, *Journal*
 14 *of Atmospheric Chemistry and Physics*, 11, 11293–11317, 2011.
 15 Holmes, C. D., Tang, Q., and Prather, M. J.: Uncertainties in climate assessment for the case of
 16 aviation NO, *Proceedings of the National Academy of Sciences, U.S.A.*, 108, 10997–11002,
 17 2011.
 18
 19 Hoor, P., Borken-Kleefeld, J., Caro, D., Dessens, O., Endresen, O., Gauss, M., Grewe, V.,
 20 Hauglustaine, D., Isaksen, I. S. A., Jöckel, P., Lelieveld, J., Meijer, E., Olivie, D., Prather, M.,
 21 Schnadt Poberaj, C., Staehelin, J., Tang, Q., van Aardenne, J., van Velthoven, P., and Sausen,
 22 R.: The impact of traffic emissions on atmospheric ozone and OH: results from QUANTIFY,
 23 *Journal of Atmospheric Chemistry and Physics*, 9, 3113-3136, 2009.
 24
 25 Horowitz, L. W., Walters, S., Mauzerall, D. L., Emmons, L. K., Rasch, P. J., Granier, C., Tie,
 26 X., Lamarque, J.-F., Schultz, M. G., Tyndall, G. S., Orlando, J. J., and Brasseur, G. P.: A
 27 global simulation of tropospheric ozone and related tracers, Description and evaluation of
 28 MOZART, version 2, *Journal of Geophysical Research*, 108, 4784, 2003.
 29

1 IPCC, 1999: Aviation and the global atmosphere, Intergovernmental Panel on Climate Change.
2 Penner, J., et al., Eds., Cambridge University Press, Cambridge, UK, 1999.

3
4 IPCC, 2001: Climate change, The scientific basis. Contribution of Working Group I to the
5 Third Assessment Report of the Intergovernmental Panel on Climate Change, Houghton, J. T.,
6 et al., Eds., Cambridge University Press, Cambridge, UK, 2001.

7
8 IPCC, 2007: Climate change, The physical science basis. Contribution of Working Group I to
9 the Fourth Assessment Report of the Intergovernmental Panel on Climate Change. Solomon, S.,
10 et al., Eds, Cambridge University Press, Cambridge, UK, 2007.

11
12 Penner, J. E., Lister, D. H., Griggs, D. J., Dokken, D. J., McFarland M., (Eds.):
13 Intergovernmental Panel on Climate Change, Aviation and the Global Atmosphere, Cambridge
14 University Press, Cambridge, UK, 1999.

15
16 Prather, M. J.: Lifetimes and eigenstates in atmospheric chemistry, Journal of Geophysical
17 Research Letter., 21, 801-4, 1994.

18
19 Isaksen, I. S. A., Granier, C., Myhre, G., Berntsen, T. K., Dalsøren, S. B., Gauss, M., Klimont,
20 Z., Benestad, R., Bousquet, P., Collins, W., Cox, T., Eyring, V., Fowler, D., Fuzzi, S., Jöckel,
21 P., Laj, P., Lohmann, U., Maione, M., Monks, P., Prevo, A. S. H., Raes, F., Richter, A.,
22 Rognerud, B., Schulz, M., Shindell, D., Stevenson, D. S., Storelvmo, T., Wang, W.-C., van
23 Weele, M., and Wuebbles, D.: Atmospheric composition change: climate–chemistry
24 interactions, Atmospheric Environment, 43, 5138-5192, 2009.

25
26 Johnson, C.: Impact of aircraft and surface emissions of nitrogen oxides on tropospheric ozone
27 and global warming, Nature, 355, 69-71, 1992.

Johnson, C. E., Derwent, R. G.: Relative radiative forcing consequences of global emissions of hydrocarbons, carbon monoxide and NO_x from human activities estimated with a zonally-averaged two-dimensional model, *Climatic Change*, 34, 439-462, 1996.

Johnston, H. S.: Reduction of stratospheric ozone by nitrogen oxide catalysts from supersonic transport exhaust, *Science*, 173, 517-522, 1971.

Kinnison, D. E., Brasseur, G. P., Walters, S., Garcia, R. R., Marsh, D. A., Sassi, F., Boville, B. A., Harvey, L., Randall, C., Emmons, L., Lamarque, J.-F., Hess, P., Orlando, J., Tyndall, G., Tie, X. X., Randel, W., Pan, L., Gettelman, A., Granier, C., Diehl, T., Niemeier, U., and Simmons, A. J.: Sensitivity of chemical tracers to meteorological parameters in the MOZART-3 chemical transport model, *Journal of Geophysical Research*, 112, D20302, doi:10.1029/2006JD007879, 2007.

Kinnison, D. E., Marsh, D. R., Garcia, R. R., Vitt, F., Tilmes, S., Mills, M. J., Lamarque, J.-F., Emmons, L. K., Orlando, J. J., Gettelman, A., Liu, H.-L., Yudin, V., Park, M., Randel, W., Pan, L. L., Brakebusch, M., Randall, C. E., and Hess, P.: Description and evaluation of the Whole Atmosphere Community Climate Model (WACCM): Chemistry Update, in preparation, 2011.

Koffi, B., Szopa, S., Cozic, A., Hauglustaine, D., and van Velthoven, P.: Present and future impact of aircraft, road traffic and shipping emissions on global tropospheric ozone, *Journal of Atmospheric Chemistry and Physics*, 10, 681-711, 2010.

Köhler, M. O., Radel, G., Dessens, O., Shine, K. P., Rogers, H. L., Wild, O., and Pyle, J. A.: Impact of perturbations to nitrogen oxide emissions from global aviation, *Journal of Geophysical Research*, 113, 2008.

Lamarque, J.-F., Emmons, L. K., Hess, P. G., Kinnison, D. E., Tilmes, V., Vitt, V., Heald, V., Holland, E. A., Lauritzen, P. H., Neu, J., Orlando, J. J., Rasch, P., and Tyndall, G.: CAM-chem: Description and evaluation of interactive atmospheric chemistry in CESM, *Geoscientific Model Development Discussions*, 5, 369 – 411, 2011.

- 1
2 Lee, D. S., Fahey, D. W., Forster, P. M., Newton, P. J., Wit, R. C. N., Lim, L. L., Owen, B.,
3 and Sausen, R.: Aviation and global climate change in the 21st century, *Atmospheric*
4 *Environment*, 43, 3520 – 3537, 2009.
- 5
6 Liang, Q., Rodriguez, J. M., Douglass, A. R., Crawford, J. H., Olson, J. R., Apel, E., Bian, H.,
7 Blake, D. R., Brune, W., Chin, M., Colarco, P. R., da Silva, A., Diskin, G. S., Duncan, B. N.,
8 Huey, L. G., Knapp, D. J., Montzka, D. D., Nielsen, J. E., Pawson, S., Riemer, D. D.,
9 Weinheimer, A. J., and Wisthaler, A.: Reactive nitrogen, ozone and ozone production in the
10 Arctic troposphere and the impact of stratosphere-troposphere exchange, *Journal of*
11 *Atmospheric Chemistry and Physics*, 11, 13181-13199, 2011.
- 12
13 Liu, X., Easter, R. C., Ghan, S. J., Zaveri, R., Rasch, P., Shi, X., Lamarque, J.-F., Gettelman,
14 A., Morrison, H., Vitt, F., Conley, A., Park, S., Neale, R., Hannay, C., Ekman, A., Hess, P.,
15 Mahowald, N., Collins, W., Iacono, M., Bretherton, C., and Flanner, M.: Toward a minimal
16 representation of aerosol direct and indirect effects: Model description and evaluation,
17 *Geoscientific Model Development Discussion*, 4, 3485-3598, doi:10.5194/gmdd-4-3485-2012,
18 2012.
- 19
20 McElroy, M. B., Wofsy, S. C., Penner, J. E., and McConnell, J. C.: Atmospheric ozone:
21 Possible impact of stratospheric aviation, *Journal of the Atmospheric Sciences*, 31, 287, 1974.
- 22
23 Meinshausen, M., Raper, S. C. B., and Wigley, T. M. L.: Emulating coupled atmosphere-ocean
24 and carbon cycle models with a simpler model, *MAGICC6 – Part 1: Model description and*
25 *calibration*, *Journal of Atmospheric Chemistry and Physics*, 11, 1417–1456, 2011.
- 26
27 Medeiros, B., Williamson, D. L., Hannay, C., and Olson, J. G.: Southeast Pacific stratocumulus
28 in the Community Atmosphere Model, *Journal of Climate*, 25, 6175–6192, 2012.

1 Morrison, H., and Gettelman, A.: A new two-moment bulk stratiform cloud microphysics
2 scheme in the NCAR Community Atmosphere Model (CAM3), Part I: Description and
3 numerical tests, *Journal of Climate*, 21, 3642–3659, 2008.

4
5 Naik, V., Voulgarakis, A., Fiore, A. M., Horowitz, L. W., Lamarque, J.-F., Lin, M., Prather, M.
6 J., Young, P. J., Bergmann, D., Cameron-Smith, P. J., Cionni, I., Collins, W. J., Dalsøren, S. B.,
7 Doherty, R., Eyring, V., Faluvegi, G., Folberth, G. A., Josse, B., Lee, Y. H., MacKenzie, I. A.,
8 Nagashima, T., van Noije, T. P. C., Plummer, D. A., Righi, M., Rumbold, S. T., Skeie, R.,
9 Shindell, D. T., Stevenson, D. S., Strode, S., Sudo, K., Szopa, S., and Zeng, G.: Preindustrial to
10 present day changes in tropospheric hydroxyl radical and methane lifetime from the
11 Atmospheric Chemistry and Climate Model Intercomparison Project (ACCMIP), *Journal of*
12 *Atmospheric Chemistry and Physics*, 13, 5277-5298, doi:10.5194/acpd-12-30755-2012, 2013.

13
14 Neale, R. B., Richter, J., Park, S., Lauritzen, P. H., Vavrus, S. J., Rasch, P. J., and Zhang, M.:
15 The mean climate of the Community Atmosphere Model (CAM4) in forced SST and fully
16 coupled experiments, *Journal of Climate*, 26, 5150-5168, DOI: 10.1175/JCLI-D-12-00236.1,
17 2013.

18
19 Neu, J. L., and Prather, M. J.: Toward a more physical representation of precipitation
20 scavenging in global chemistry models: cloud overlap and ice physics and their impact on
21 tropospheric ozone. *Journal of Atmospheric Chemistry and Physics Discussions*, 11, 24413–
22 24466, 2011.

23
24 Olsen, S. C., and Wuebbles, D. J.: Comparison of global 3-D aviation emissions datasets,
25 *Journal of Atmospheric Chemistry and Physics*, 12, 16885 – 16992, 2012.

26
27 Olsen, S. C., Brasseur, G. P., Wuebbles, D. J., Barrett, S., Dang, H., Eastham, S. D., Jacobson,
28 M. Z., Khodayari, A., Selkirk, H., Sokolov, A., Unger N.: Comparison of model estimates of
29 the effects of aviation emissions on atmospheric ozone and methane, *Geophysical Research*
30 *Letters*, accepted, 2013.

1
2 Patten, K. O., Khamaganov, V. G., Orkin, V. L., Baughcum, S. L., Wuebbles, D. J.: OH
3 reaction rate constant, IR absorption spectrum, ozone depletion potentials and global warming
4 potentials of 2-bromo-3,3,3-trifluoropropene, Journal of Geophysical Research, 116, D24307.
5 2011.

6
7 Price, C., Penner, J., and Prather, M.: NO_x from lightning: Global distribution based on
8 lightning physics, Geophysical Research Letter, Res., 102, 5929–5941, 1997.

9
10 Ridley, B., Pickering, K., and Dye, J.: Comments on the parameterization of lightning-
11 produced NO in global chemistry-transport models, Atmospheric Environment, 39, 6184–6187,
12 2005.

13
14 Rienecker, M. M., et al (2008), The GEOS-5 Data Assimilation System-Documentation
15 of versions 5.0.1, 5.1.0, and 5.2.0.NASA/TM-2008-104606, Vol. 27, Technical Report Series
16 on Global Modeling and Data Assimilation, 118 pp. (available at
17 <http://gmao.gsfc.nasa.gov/systems/geos5/>)

18
19 Roof, C., Hansen, A., Fleming, G. G., Thrasher, T., Nguyen, A., Hall, C., Dinges, E., Bea, R.,
20 Grandi, F., Kim, B. Y., Usdrowski, S., and Hollingsworth, P.: Aviation Environmental Design
21 Tool (AEDT) System Architecture, Doc #AEDTAD-01, USDOT Volpe Center and CSSI Inc.
22 and ATAC Inc. and Wyle Laboratories Inc. and Georgia Tech, Cambridge, MA, 2007.

23
24 Sillman, S., 2012. Overview: Tropospheric ozone, smog and ozone-NO_x-VOC sensitivity.
25 [online] University of Michigan. Available from: [http://www-](http://www-personal.umich.edu/~sillman/Sillman-webOZONE.pdf)
26 [personal.umich.edu/~sillman/Sillman-webOZONE.pdf](http://www-personal.umich.edu/~sillman/Sillman-webOZONE.pdf) [Accessed 11 April 2012].

27
28 Spivakovsky, C. M., Logan, J. A., Montzka, S. A., Balkanski, Y. J., Foreman-Fowler, M.,
29 Jones, D. B. A., Horowitz, L. W., Fusco, A. C., Brenninkmeijer, C. A. M., Prather M. J.,
30 Wofsy, S. C., and McElroy, M. B.: Three-dimensional climatological distribution of

1 tropospheric OH: Update and evaluation, *J. Geophys. Res.*, 105, 8931–8980,
2 doi:[10.1029/1999JD901006](https://doi.org/10.1029/1999JD901006), 2000.

3
4 Stevenson, D. S., and Derwent, R. G.: Does the location of aircraft nitrogen oxide emissions
5 affect their climate impact? *Geophysical Research Letters* 36.17, L17810, 2009.

6
7 Stevenson, D. S., Doherty, R. M., Sanderson, M. G., Collins, W. J., Johnson, C. E., and
8 Derwent, R. G.: Radiative forcing from aircraft NO_x emissions: Mechanisms and seasonal
9 dependence, *Journal of Geophysical Research*, 109, 2004.

10
11 Stevenson, D. S., Dentener, F. J., Schultz, M. G., et al.: Multi-model ensemble simulations of
12 present-day and near future tropospheric ozone, *Journal of Geophysical Research*, 111,
13 D08301, doi:[10.1029/2005JD006338](https://doi.org/10.1029/2005JD006338), 2006.

14
15 Tilmes, S., Lamarque, J.-F., Emmons, L. K., Conley, A., Schultz, M. G., Saunio, M., Thouret,
16 V., Thompson, A. M., Oltmans, S. J., Johnson, B., and Tarasick, D.: Technical Note:
17 Ozone sonde climatology between 1995 and 2011: Description, Evaluation and Applications,
18 *Atmospheric Chemistry and Physics*, 12, 7475–7497, doi:[10.5194/acp-12-7475-2012](https://doi.org/10.5194/acp-12-7475-2012), 2012.

19 Voulgarakis, A., Savage, N. H., Wild, O., Carver, G. D., Clemitshaw, K. C., and Pyle, J. A.:
20 Upgrading photolysis in the p-TOMCAT CTM: model evaluation and assessment of the role of
21 clouds, *Geoscientific Model Development*, 2, 59–72, 2009.

22
23 Tilmes, S., Lamarque, J.-F., Emmons, L. K., Kinnison, D. E., Bardeen, C., Deeter, M., Vitt, F.:
24 Representation of chemistry in CAM4 and CAM5 in the Community Earth System Model
25 (CESM1.2), in preparation.

26
27 Voulgarakis, A., Naik, V., Lamarque, J.-F., Shindell, D. T., Young, P. J., Prather, M. J., Wild,
28 O., Field, R. D., Bergmann, D., Cameron-Smith, P., Cionni, I., Collins, W. J., Dalsøren, S. B.,
29 Doherty, R. M., Eyring, V., Faluvegi, G., Folberth, G. A., Horowitz, L. W., Josse, B.,
30 MacKenzie, I. A., Nagashima, T., Plummer, D. A., Righi, M., Rumbold, S. T., Stevenson, D.

1 S., Strode, S. A., Sudo, K., Szopa, S., and Zeng, G.: Analysis of present day and future OH and
2 methane lifetime in the ACCMIP simulations, *Journal of Atmospheric Chemistry and Physics*,
3 13, 2563–2587, doi:10.5194/acp-13-2563- 2013, 2013.

4
5
6 Walcek, C. J., Brost, R. A., Chang, J. S., and Wesely, M. L.: SO₂, sulfate and HNO₃ deposition
7 velocities computed using regional land use and meteorological data, *Atmospheric*
8 *Environment*, 20, 946–964, 1986.

9
10 Walmsley, J. L. and Wesely, M. L.: Modification of coded parameterizations of surface
11 resistances to gaseous dry deposition, *Atmospheric Environment*, 30, 1181–1188, 1996.

12
13 Wesely, M. L. and Hicks, B. B.: A review of the current status of knowledge on dry deposition,
14 *Atmospheric Environment*, 34, 2261–2282, 2000.

15
16 Wild, O., Prather, M. J., and Akimoto, H.: Indirect long-term global cooling from NO_x
17 emissions, *Geophysical Research Letters*, 28, 1719-1722, 2001.

18
19 Wilkerson, J.T., Jacobson, M. Z., Malwitz, A., Balasubramanian, S., Wayson, R., Fleming, G.,
20 Naiman, A. D., and Lele, S. K.: Analysis of emission data from global commercial aviation:
21 2004 and 2006, *Journal of Atmospheric Chemistry and Physics*, 10, 6391–6408, 2010.

Table 1. Annual tropospheric mean burden of HOx, NOx, gaseous NOy and the ratios of OH : HO₂ and NOx : NOy in both CAM5 and CAM4 for both the control run (_c) and aviation NOx-perturbed run (_p).

	O ₃ (kg)	OH (kg)	HO ₂ (kg)	HOx (kg)	OH/HO ₂	NOx (kgN)	NOy (kgN)	NOx/NOy
CAM4_c	3.71e+11	2.11E+05	2.59E+07	2.61E+07	8.15E-03	1.20E+08	7.69E+08	0.156
CAM4_p	3.79e+11	2.17E+05	2.58E+07	2.60E+07	8.39E-03	1.24E+08	7.96E+08	0.156
CAM5_c	3.41e+11	2.68E+05	2.73E+07	2.76E+07	9.82E-03	1.24E+08	7.30E+08	0.170
CAM5_p	3.50e+11	2.75E+05	2.72E+07	2.75E+07	1.01E-02	1.29E+08	7.73E+08	0.167

Table 2. Global annual average CH₄ lifetimes against reaction with OH, as calculated by CAM4 and CAM5 for the control run and for the NOx perturbation run. The relative change between runs is displayed in the right-most column. It is noted that the calculated lifetimes are shorter than the CH₄ lifetime derived based on Methyl chloroform analysis (Prather et al., 2012).

CH ₄ lifetime (yr)	Control run	Perturbed run	Rel change (%)
CAM5	7.09	6.97	1.69
CAM4	8.83	8.71	1.40

Comparison to Ozonesondes

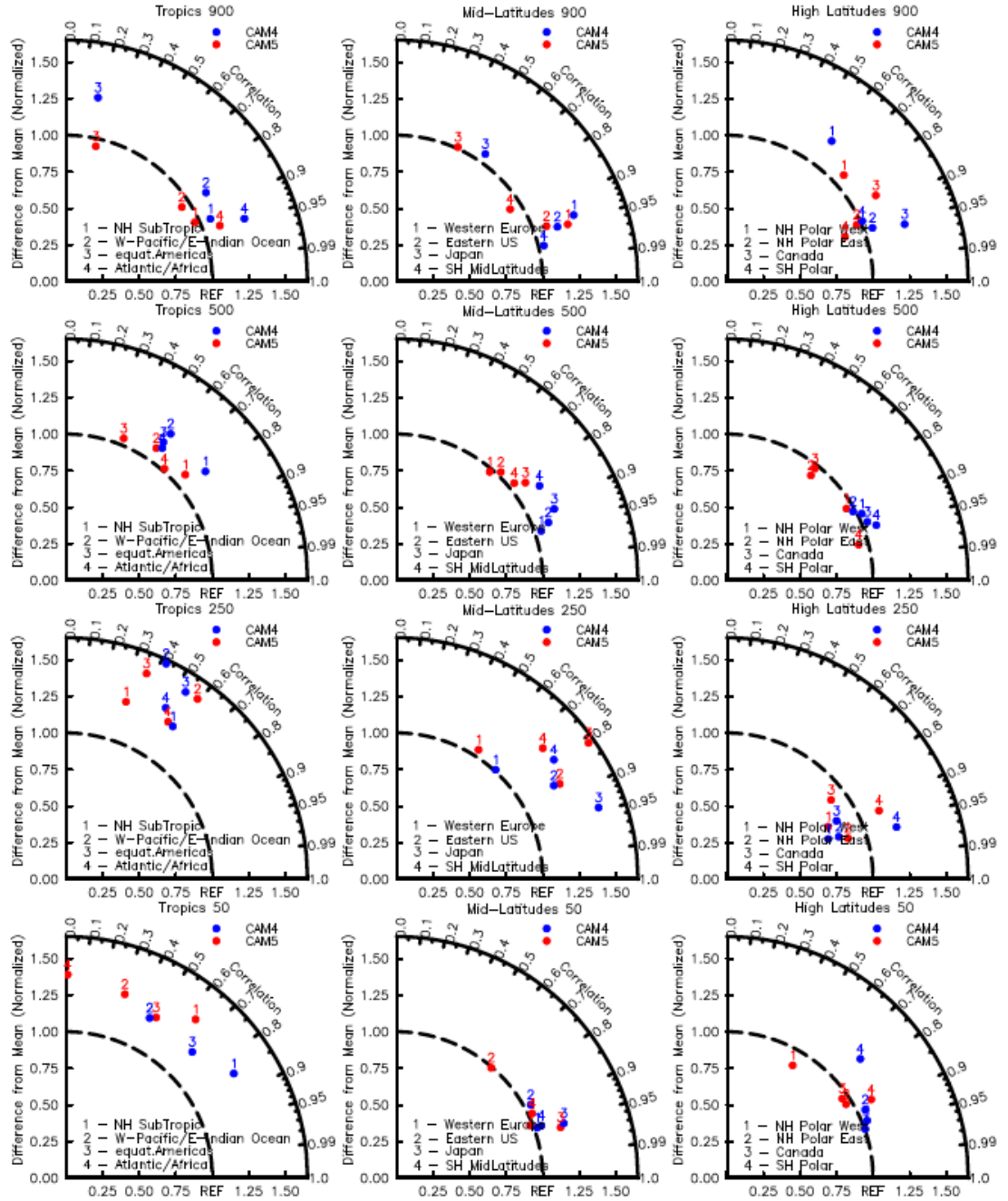


Figure 1. Taylor diagram of modeled background ozone from the control runs against ozonesonde climatology for four pressure levels and three latitudinal regions. REF along the abscissa denotes the observations while the radial distance describes the normalized bias. The correlation for the seasonal cycle is described along the angle.

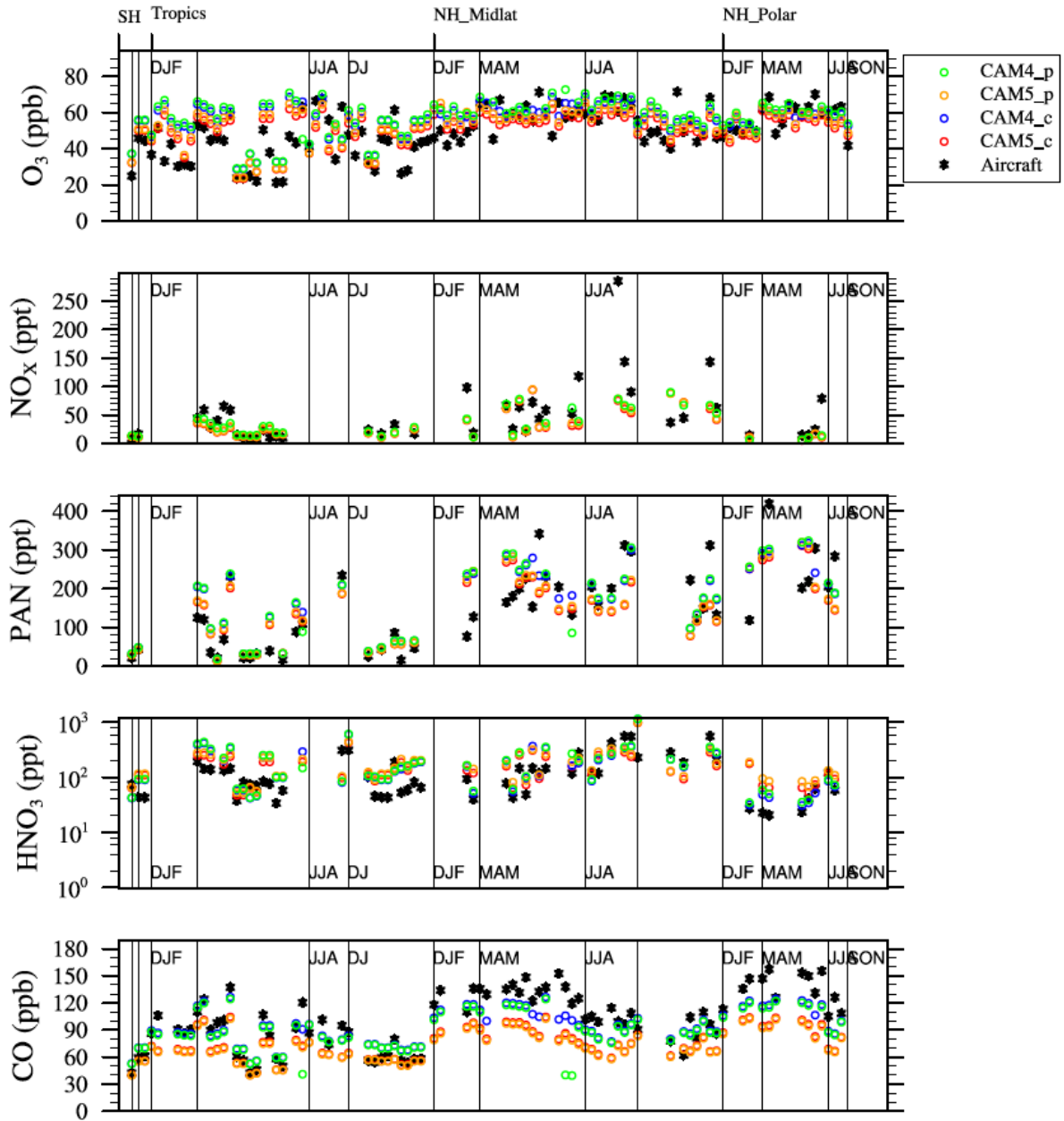


Figure 2. Comparison between aircraft observations over different regions and seasons and different model simulation, averaged between 2-7km, for Ozone, NO_x, PAN, HNO₃, and CO, based on an updated version of the aircraft climatology by Emmons et al., 2000, as described in detail in Tilmes et al., 2014 (in preparation).

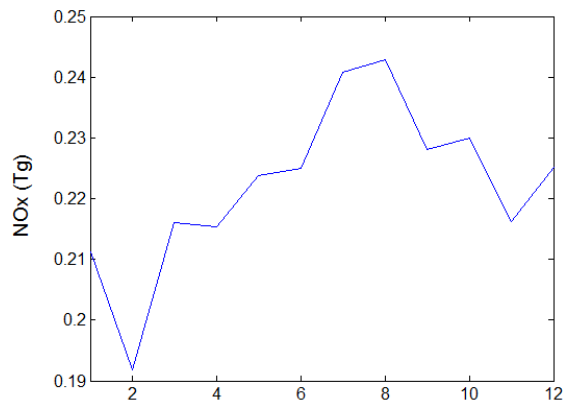
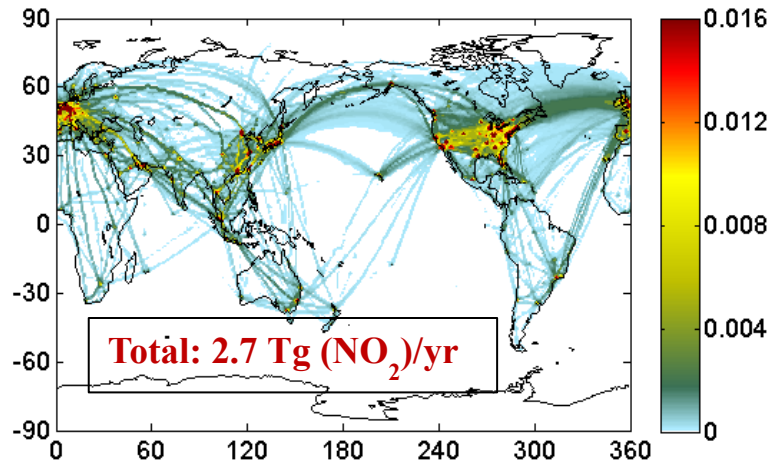


Figure 3. Spatial distribution of vertically-integrated aviation NO_x emissions for 2006.

Figure 4. Seasonal distribution of global aviation NO_x emissions for 2006.

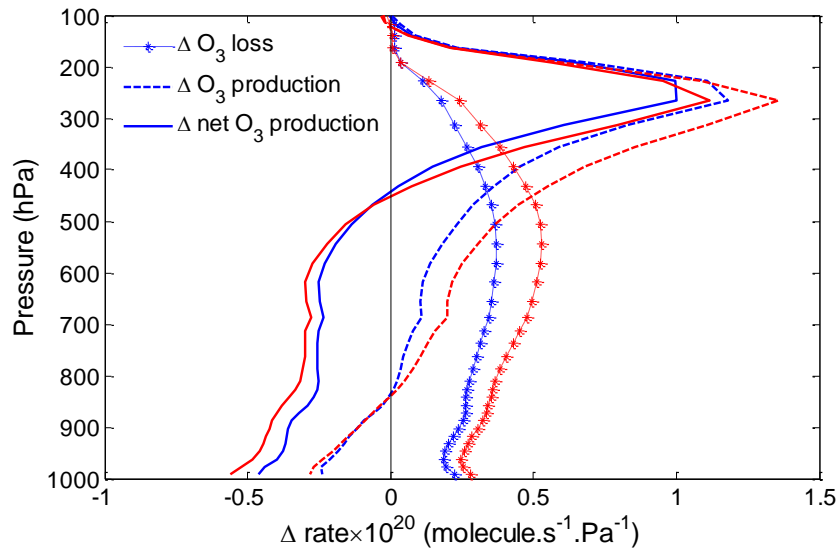


Figure 5. Vertical profile describing the aviation NO_x-induced change in the rate of O₃ production with height (results are shown in red for CAM5 and in blue for CAM4). Net rate of ozone production (solid line), the gross rate of ozone production (dashed line), and the rate of ozone loss (dotted line) are shown. Production and loss rates are calculated as zonal and meridional means.

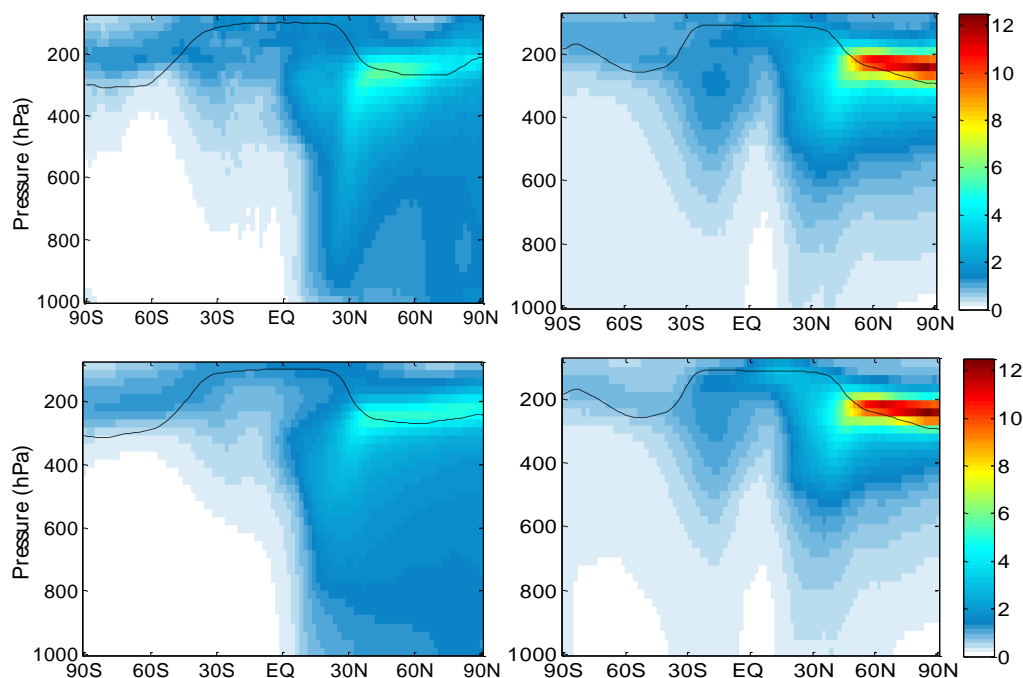


Figure 6. Zonal mean perturbations of ozone (ppb) during January (left) and July (right). CAM5 is in the top panel, while CAM4 is on the bottom. The dashed line indicates the tropopause.

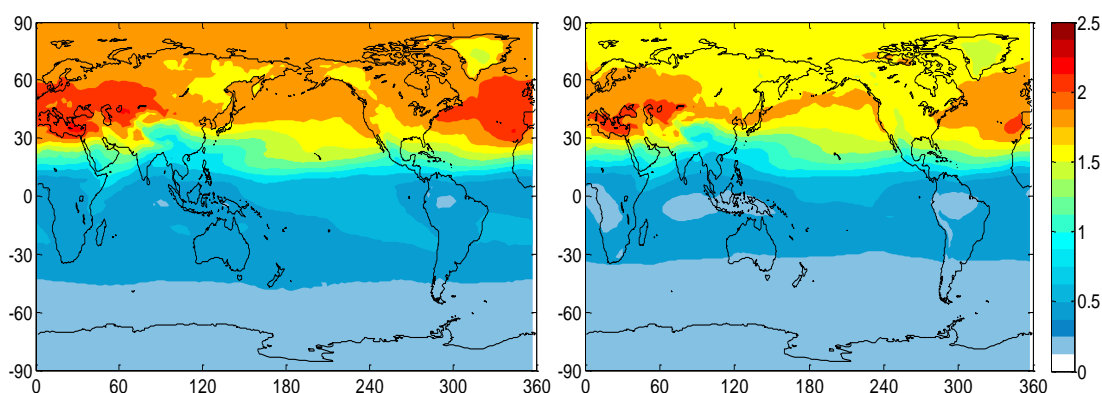


Figure 7. Yearly mean perturbations of the ozone column (Δ DU) based on 2006 aircraft NO_x emissions. CAM5 is on the left, while CAM4 is on the right.

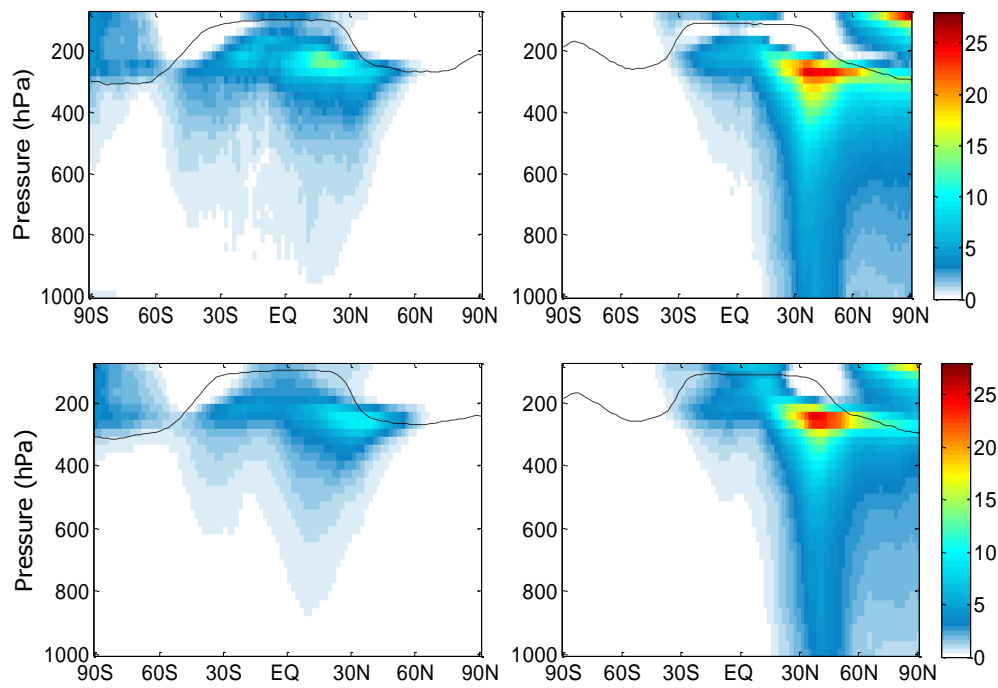


Figure 8. Aviation induced OH perturbations ($10^{-4} \Delta\text{molec cm}^{-3}$) during January (left) and July (right). CAM5 is in the top panel, while CAM4 is in the bottom. The dashed line indicates the tropopause.

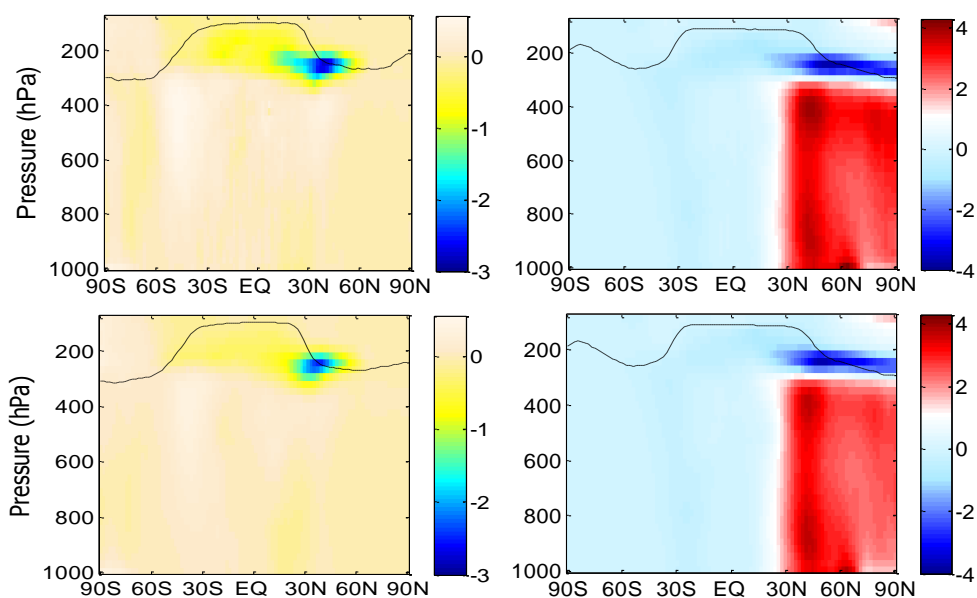


Figure 9. As in Figure 7, but for HO_2 ($10^{-6} \Delta \text{molec cm}^{-3}$).

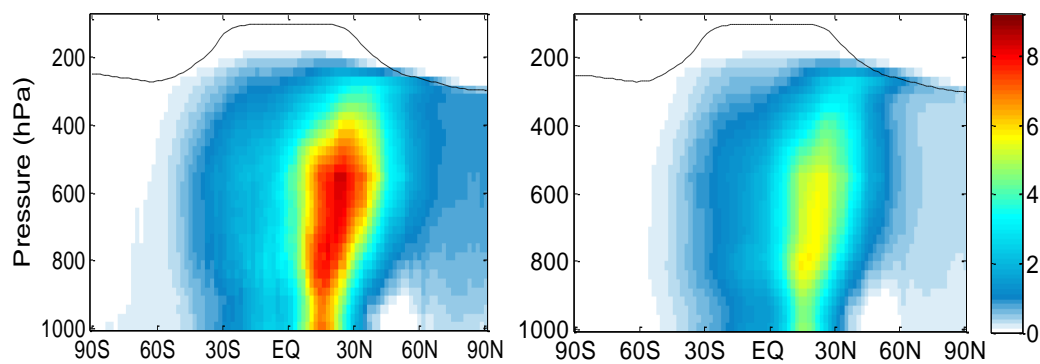


Figure 10. Annual zonal averaged CH_4 loss ($10^{-3} \Delta \text{molec cm}^{-3} \text{s}$) induced by aviation NO_x emissions. CAM5 is on the left, CAM4 is on the right. The dashed line indicates the tropopause.

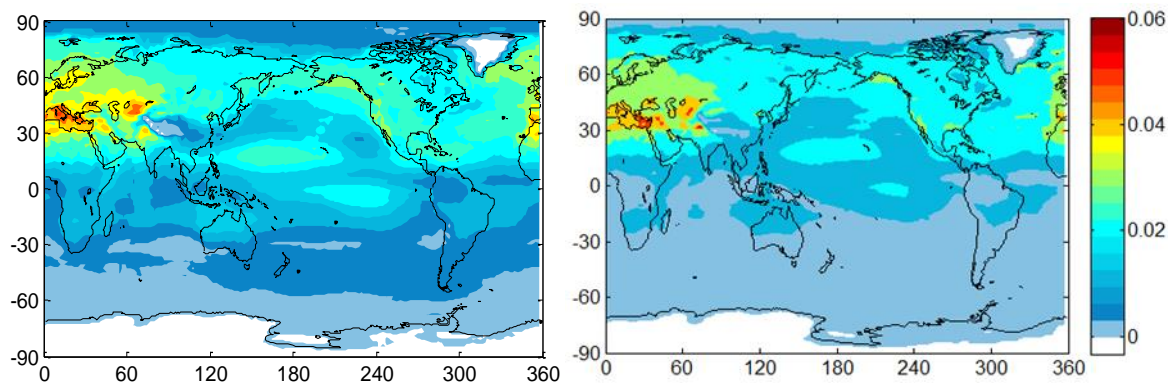


Figure 11. Yearly mean radiative forcing (mWm^{-2}) from O_3 due to aviation NO_x emissions. CAM5 is on the left, CAM4 is on the right.